13th International Symposium on Turbulence and Shear Flow Phenomena (TSFP13)
Montreal, Canada, June 25–28, 2024

EFFECTS OF ROUGHNESS HEIGHT COMPOSITION ON TURBULENCE CHARACTERISTICS IN TURBULENT BOUNDARY LAYERS

Setyo Nugroho
School of Electrical and Mechanical Engineering
The University of Adelaide
Adelaide, 5000, South Australia, Australia
setyo.nugroho@adeleide.edu.au

Bagus Nugroho
Department of Mechanical Engineering
The University of Melbourne
Melbourne, 3001, Victoria, Australia
bagus.nugroho@unimelb.edu.au

Eric Fusil
School of Electrical and Mechanical Engineering
The University of Adelaide
Adelaide, 5000, South Australia, Australia
eric.fusil@adeleide.edu.au

Rey Chin
School of Electrical and Mechanical Engineering
The University of Adelaide
Adelaide, 5000, South Australia, Australia
rey.chin@adeleide.edu.au

ABSTRACT

Turbulence characteristics play a crucial role in generating drag on the hull of a bio-fouled ship. Experiments in a wind tunnel using hot-wire anemometry were conducted to investigate this. The rough surfaces were made by randomly distributing two different mixtures of sand grains with an average height of 0.9 mm, covering 10%, 30%, 50%, 70%, and 100% of a flat plate surface. This study aims to establish a correlation between the extent of surface roughness and the distribution of roughness heights to turbulence characteristics, including the Hama roughness function. The results indicate an increase in the Hama roughness function as roughness area coverage increases and reaches a peak value at 50% roughness area coverage. Furthermore, the Hama roughness function decreases and stagnates at higher roughness area coverage. Interestingly, turbulence intensity remains relatively constant across different sand mixture compositions when the area coverage matches, indicating that the height composition does not significantly affect the turbulence intensities.

INTRODUCTION

Wall-bounded turbulent flow over rough surfaces has received much attention due to its significant role in applied engineering, such as bio-fouled ship-hulls. On a rough wall boundary layer, the streamwise mean velocity profile experiences a downward shift by a value represented by the Hama roughness function, ΔU^+ (Hama, 1954). This alteration in the velocity profile leads to an elevation in frictional resistance because of the momentum loss. The streamwise mean velocity profile can be written in the following equation:

$$U^+ = \frac{1}{\kappa} \ln y_*^+ + A - \Delta U^+, \tag{1}$$

here the von Karman constant, $\kappa = 0.39$, the smooth wall intercept, $A = 4.3$. The non-dimensional velocity in the boundary layer is denoted as U^+, and the non-dimensional normal distance from the wall is represented as y_*^+. These terms are further defined as follows: $U^+ = \frac{U}{U_\tau}$ and $y_*^+ = \frac{(y+\varepsilon)U_\tau}{\nu}$, where U is the mean velocity. U_τ is the friction velocity defined as $\sqrt{\frac{\tau_w}{\rho}}$, y is the normal distance from the wall, ε is the zero-plane origin, ν is the kinematic viscosity, τ_w is the shear stress magnitude, and ρ is the density of the fluid. In this paper, Reynolds number is defined as $Re_\tau = \frac{\delta U_\tau}{\nu}$, where δ is the boundary layer thickness. The Hama roughness function, ΔU^+, illustrates the downward shift in the mean velocity profile caused by surface roughness. In essence, ΔU^+ quantifies the differences between velocity profiles on smooth and rough surfaces. Consequently, ΔU^+ equals zero for a smooth wall.

While there has been significant research on uniform roughness height and shape, it is important to comprehend how roughness coverage and size distribution impact the Hama roughness function and turbulence intensities. Investigations into the effects of varying roughness size and coverage are infrequent, and when conducted, they typically involve synthetic roughness with controlled sizes, e.g. cube (Leonardi & Castro, 2010), sinusoidal wave (MacDonald *et al.*, 2016), truncated cone (Sarakinos & Busse, 2022; Womack *et al.*, 2022), and hemispheres (Nugroho *et al.*, 2023). Their findings consistently show that there is a peak in ΔU^+ value at specific levels of roughness area coverage. Roughness size and coverage can profoundly influence the effective roughness properties, the development of the boundary layer, and the interaction between the flow and the rough surface.

From those earlier investigations, it is imperative to conduct further research to quantify and fully understand the implications of roughness coverage and size distribution. This will contribute to a more comprehensive understanding of turbulent flow over wall-bounded rough surfaces. This paper discusses turbulent boundary layer (TBL) over sand-grain roughness with varying coverage areas of rough surfaces, aiming to explore the relationship between turbulence characteristics and the extent of surface roughness coverage. The Hama roughness function was determined by experimentally examining the flow over various coverage areas using a wind tunnel and hot-wire anemometry (HWA).

EXPERIMENT SETUP

The experiments were conducted in a closed-loop wind tunnel at the University of Adelaide. The wind tunnel is equipped with a test section that spans 2000 mm in length and a rectangular cross-sectional area with a size of 500 by 300 mm. Single-wire boundary-type probes were employed and operated by an in-house designed Melbourne University Constant Temperature Anemometer (MUCTA) to conduct the measurements. The layout of the wind tunnel is illustrated in figure 1. Measurements were conducted using single-wire boundary-type probes featuring prong tips 2 mm apart. Platinum-Wollaston wires were attached to these tips, and subsequent etching resulted in a sensor filament characterized by a diameter (d) of 2.5 μm and a length (l) of 0.5 mm. The length-to-diameter ratio (l/d) was around 200, a value deemed appropriate for reducing attenuation arising from end conduction, as suggested by Ligrani & Bradshaw (1987) andHutchins *et al.* (2009). The inner-scaled wire length, $l^+ = lU_\tau/\nu$, will exhibit a range from 15 to 36. This variability in spatial resolution suggests that the near-wall measurements might undergo some degree of attenuation due to restricted spatial resolution, particularly at higher free-stream velocities, as discussed by Hutchins *et al.* (2009). The system's frequency response was fine-tuned to around 14.2 kHz when the probes experienced zero free-stream flow. This adjustment ensures the anemometer can accurately record velocity fluctuations in turbulent flow. The hot-wire analog output was captured using an acquisition board, specifically the USB-NI9324. The data acquisition system operated at a frequency of 51,200 Hz, and each sampling session lasted for 120 seconds. Fifty measurement points, logarithmically distributed along the wall-normal direction, were recorded for each boundary layer measurement.

The hot-wire sensors employed in the experiments underwent in situ calibration against a Pitot-static tube. To accommodate the experiment setup, which was conducted at 10 m/s and 20 m/s free-stream velocities, the calibration involved varying the wind tunnel speed across a range of velocities, typically from zero to 22 m/s. Calibrations were conducted before and after each wall-normal boundary layer traverse to detect potential hot-wire voltage drifting and ensure measurement accuracy. The free-stream velocity was determined by calculating the difference between the total and static pressures obtained from the Pitot tube, monitored using an electronic barometer (220DD Barotron, MKS). Concurrently, the flow temperature was observed through a calibrated RTD-type thermocouple (PT1000). Throughout each traverse station, the free-stream velocity was continuously recorded and compared with the hot-wire signals in the free-stream flow. To precisely determine the offset distance of the hot wire from the rough wall at the initial measurement point in the turbulent boundary layer (TBL), a high-magnification digital microscope was utilized to monitor the distance between the probe's tip and the wall.

The rough surfaces were made involving the following steps: firstly, the three-dimensional roughness was produced using sand grains with two different mixture compositions - a ratio of 1:1 for sizes 0.6 mm and 1.2 mm on average and a ratio of 1:2:1 for sizes 0.6 mm, 0.9 mm, and 1.2 mm on average. The sand dimensions were chosen so that each mixture would have a height average of 0.9 mm. These mixtures were then applied to cover surface area percentages of 10%, 30%, 50%, 70%, and 100% on a flat plate, representing the progression of biofouling growth on a ship-hull surface. Subsequently, a random distribution of sand grains on the surface was performed to mimic a natural roughness pattern.

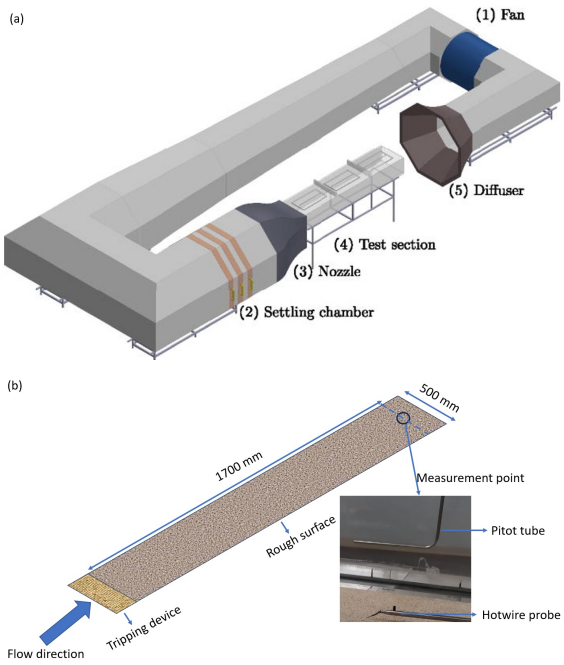

Figure 1. (a) Layout of wind tunnel apparatus Abdelaziz *et al.* (2023), (b) Layout of measurement setup

Estimating friction velocity U_τ

Determining the skin-friction velocity U_τ on a rough surface poses increased challenges, incorporating two crucial components: ΔU^+ and zero-plane origin, ε (Hama, 1954; Perry *et al.*, 1969; Schultz & Myers, 2003; Squire *et al.*, 2016). The conventional approach for obtaining U_τ, ε, and ΔU^+ in rough-walled flow involves the modified Clauser method (Clauser, 1954; Perry & Joubert, 1963; Flack & Schultz, 2014; Monty *et al.*, 2016). While the modified Clauser method is a widely used technique for estimating U_τ, it is crucial to recognize its limitations in terms of accuracy, particularly in estimating the logarithmic region's range. Some studies report errors of 3%-5% for U_τ (Flack *et al.*, 2007; Schultz & Myers, 2003). A recent study by Medjnoun *et al.* (2018) suggests that different measurement techniques and analyses for rough wall flow may result in varying accuracies, with variations reaching up to 15%. Therefore, caution is required when estimating U_τ in turbulent flow over rough surfaces.

Apart from U_τ, another unknown component is the zero-plane origin, ε. This parameter accounts for the flow displacement caused by roughness elements on the wall. The ε value should fall between zero and the maximum roughness height, providing a good agreement between the outer region mean velocity profile and the velocity defect law. Optimisation of ε is needed for a robust collapse between the mean velocity profile and the logarithmic line of U_τ/U_e, especially in the near-wall region (Perry & Li, 1990). The selected ε value is then incorporated into $y_* = (y + \varepsilon)$, and the inner-scaled wall-normal location, i.e., y_*, and the outer-scaled wall-normal location, i.e., y_*/δ.

RESULTS AND DISCUSSION

The experiments were carried out for all roughness configurations at two nominal free-stream velocities, 10 m/s and 20 m/s. The summary of the experimental results are presented in table 1.

Table 1. Summary of experimental results on rough surfaces.

Surface	U_∞	U_τ	ε	δ	Re_τ	$\frac{\delta}{k}$	ΔU^+	k_s	k_s^+	l^+
	ms^{-1}	ms^{-1}	mm	mm				mm		
Smooth	9.9	0.408	-	42.9	924	-	-	-	-	13.7
Smooth	19.6	0.752	-	42.9	1766	-	-	-	-	25.6
1:1 10%	9.9	0.447	0.4	48.0	1174	53.3	2.80	0.7	23.4	15.2
1:1 30%	10.0	0.476	0.6	51.0	1641	56.6	5.55	2.0	66.1	16.2
1:1 50%	9.9	0.496	0.8	51.2	1636	56.8	6.42	2.1	70.7	16.8
1:1 70%	9.9	0.472	0.8	51.4	1603	57.1	5.53	1.8	57.8	16.1
1:1 100%	9.8	0.468	0.8	50.9	1628	56.5	5.65	1.9	61.3	15.9
1:1 10%	19.6	0.932	0.4	48.5	2356	53.8	5.63	0.7	48.2	31.7
1:1 30%	19.7	0.985	0.7	52.0	3265	57.7	8.24	2.0	133.5	33.5
1:1 50%	19.5	0.975	0.8	52.5	3367	58.3	8.35	2.1	139.5	34.4
1:1 70%	19.5	0.973	0.8	52.0	3140	57.7	7.94	1.8	119.0	33.2
1:1 100%	19.4	0.968	0.8	51.7	3237	57.4	8.15	1.9	129.1	33.1
1:2:1 10%	9.9	0.448	0.6	49.7	1307	55.2	2.73	0.5	15.0	15.2
1:2:1 30%	9.8	0.494	0.6	51.9	1675	54.0	6.12	1.9	65.1	16.8
1:2:1 50%	9.9	0.496	0.6	51.0	1550	57.6	6.51	2.0	69.2	16.8
1:2:1 70%	9.9	0.496	0.6	51.6	1737	57.3	6.25	1.8	59.5	16.8
1:2:1 100%	9.9	0.473	0.6	51.3	1524	57.0	5.79	1.8	58.6	16.1
1:2:1 10%	19.6	0.934	0.5	50.7	2697	56.3	4.48	0.5	30.8	31.8
1:2:1 30%	19.5	0.977	0.6	51.7	3109	57.4	8.12	1.9	127.6	33.2
1:2:1 50%	19.4	0.972	0.6	52.4	3187	58.2	8.30	2.0	136.8	33.1
1:2:1 70%	19.4	0.969	0.8	52.1	3399	57.8	7.88	1.8	116.1	33.0
1:2:1 100%	19.7	0.984	0.6	52.3	3224	58.1	7.98	1.8	120.9	33.4

Streamwise mean velocity profile

To investigate the effect of area coverage, inner-normalised mean streamwise velocity profiles above the rough wall were plotted in figure 2. The results in figure 2 suggest that the slope of a log-linear region for all profiles is closely similar to the logarithmic slope observed in the data for smooth walls. Additionally, the results confirm the widely recognized effect: the presence of a rough wall induces ΔU^+ in the inner-normalised mean streamwise velocity because of the increased drag above the rough wall compared to a smooth wall's drag, leading to an augmented momentum flux toward the wall. Notably, the zero origins for the rough walls vary with the height of the non-uniform roughness. As a result, the near-wall characteristics of the streamwise mean velocity profiles differ in each case.

Figure 3 indicates that there is a noticeable increase in ΔU^+ as the roughness coverage increases from 10% to 50%, and ΔU^+ reaches its peak value at 50% roughness area coverage. Interestingly, beyond the 50% coverage, the ΔU^+ value starts to stagnate. Furthermore, for the 70% and 100% area coverage cases, the ΔU^+ decreases, and the profiles shifted slightly further up. This trend similar to the findings in Sarakinos & Busse (2022), Womack *et al.* (2022), and Nugroho *et al.* (2023). They used a regular roughness shape and observed the peak of ΔU^+ at 60%, 39%, and 30% of the roughness area coverage, respectively. Furthermore, our study shows a more significant increase in ΔU^+ at 10% roughness area coverage to 30% roughness area coverage compared to the other case. This result was also observed in the DNS results by Womack *et al.* (2022) and suggests that the low roughness area coverage effect needs to be further explored.

Hama roughness function versus roughness coverage

As previously mentioned, there is a peak of ΔU^+ in terms of increasing roughness coverage area. Figure 3 depicts the details of this relation. The plot shown in figure 3 shows a saturation value of ΔU^+ at roughness area coverage higher than 50%, similar to a study from Napoli *et al.* (2008). Their report explains this saturation phenomenon, attributing it to the irregular geometry of the rough surface, which diminishes the mutual sheltering effect typically associated with individual corrugations. The sheltering effect arises when the local topography obstructs or shields a region from direct interaction with the flow. Therefore, the stronger the mutual sheltering effect, the greater the reduction in drag. Additionally, Napoli

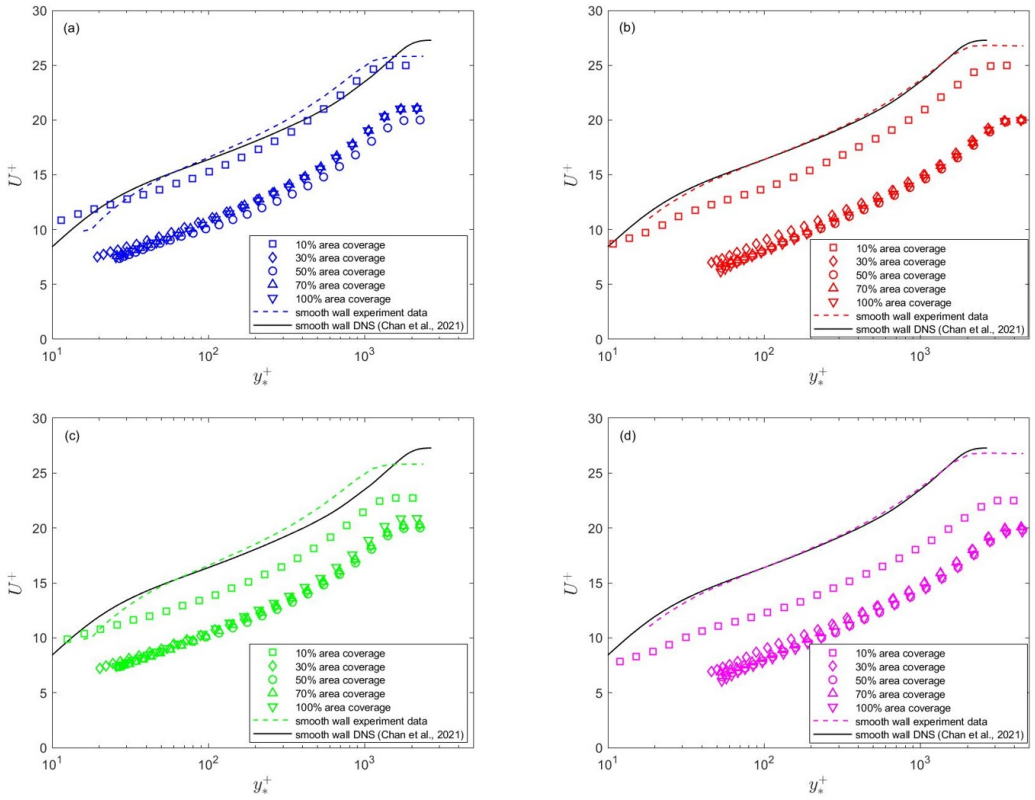

Figure 2. Comparison of rough surfaces and smooth wall TBLs. Streamwise mean velocity profile at roughness composition height; (a) 1:1 $Re_\tau \approx 1500$, (b) 1:1 $Re_\tau \approx 3200$, (c) 1:2:1 $Re_\tau \approx 1500$, and (d) 1:2:1 $Re_\tau \approx 3200$.

et al. (2008) noted a consistent pressure and friction drag ratio value when roughness area coverage is higher than 20%. Furthermore, figure 3 suggests that at 20 m/s and area coverage higher than 30%, the size distribution does not affect the ΔU^+. However, studies using a higher variance of roughness height, e.g., using sand grains with sizes 0.4 mm and 1.6 mm, need to be undertaken to verify this hypothesis.

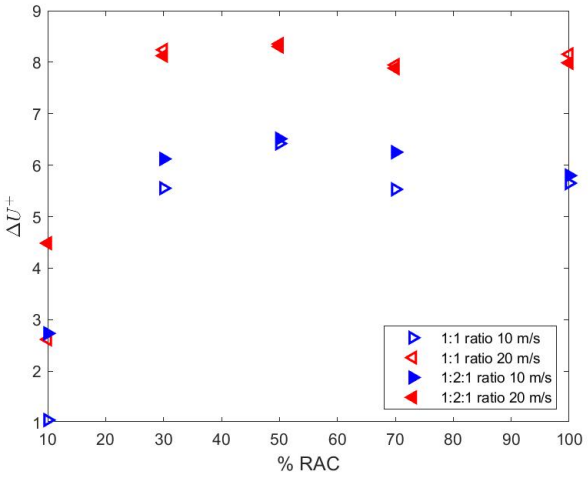

Figure 3. Hama roughness function on rough surfaces against the % roughness area coverage.

Turbulent intensity

Figure 4 shows the distribution of u'^+, the streamwise root-mean-square (r.m.s.) velocity fluctuation normalised by U_τ, in wall-normal direction. In the case of rough-wall turbulent boundary layers (TBLs), there is a decrease in normalised turbulence intensity at $y_*^+ < 30$ if compared to the smooth-wall turbulence intensity. This reduction is typically ascribed to the disruption of the near-wall cycle caused by the presence of surface roughness. Notably, the data presented here are gathered from diverse zero origins and are influenced by the local topography of the roughness surrounding the hot-wire probe. For all roughness coverage and mixture ratio composition, as Re_τ increases, the turbulence intensity at the outer region increases, indicating typical behavior of Re_τ influence. As a general trend, the composition of roughness heights does not seem to influence the turbulence intensity profile substantially. From the middle of the log region to the wake region, there are minimal differences in the magnitude of turbulence intensity among the different roughness area coverage values; they essentially collapse with each other. This occurrence can be attributed to the nearly identical Re_τ values because of similar average roughness height. Therefore, the sand composition has no significant effect on the turbulence intensities. Again, more study using a higher range of the sand size would be important to verify our finding.

CONCLUSION

Wind tunnel experiments were conducted on rough wall TBL employing HWA. The rough surfaces featured randomly distributed sand-grain roughness, encompassing two distinct sand-size compositions with similar average roughness heights and varying surface area coverage. A consistent observation in

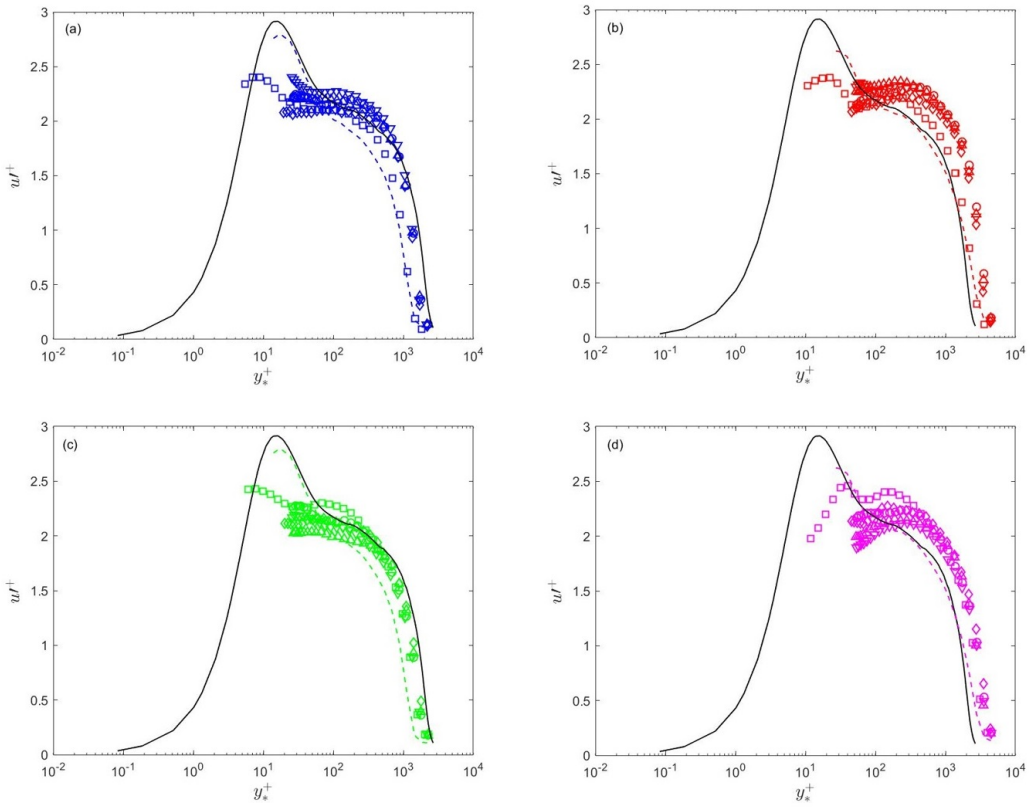

Figure 4. Comparison of rough surfaces and smooth wall TBLs. Turbulence intensities at roughness composition height; (a) 1:1 $Re_\tau \approx 1500$, (b) 1:1 $Re_\tau \approx 3200$, (c) 1:2:1 $Re_\tau \approx 1500$, and (d) 1:2:1 $Re_\tau \approx 3200$

the TBL revealed a peak Hama roughness function occurring at 50% of the roughness area coverage across different compositions and free-stream velocities. In terms of turbulence intensity profile, the roughness area coverage does not appear to have a significant effect on the outer layer. Furthermore, the sand composition does not affect the turbulence intensities in a similar roughness height case. Therefore, it is interesting to expand this study to a higher variance of sand size.

ACKNOWLEDGEMENTS

This study was financially supported by the Indonesian Endowment Fund for Education (LPDP) of the Ministry of Finance, Republic of Indonesia.

REFERENCES

Abdelaziz, Misarah, Djenidi, L, Ghayesh, Mergen H & Chin, Rey 2023 Influence of skewed three-dimensional sinusoidal surface roughness on turbulent boundary layers. *Physics of Fluids* **35** (5).

Clauser, Francis H 1954 Turbulent boundary layers in adverse pressure gradients. *Journal of the Aeronautical Sciences* **21** (2), 91–108.

Flack, KA, Schultz, MP & Connelly, JS 2007 Examination of a critical roughness height for outer layer similarity. *Physics of Fluids* **19** (9), 095104.

Flack, Karen A & Schultz, Michael P 2014 Roughness effects on wall-bounded turbulent flows. *Physics of Fluids* **26** (10), 101305.

Hama, Francis R 1954 Boundary layer characteristics for smooth and rough surfaces. *Trans. Soc. Nav. Arch. Marine Engrs.* **62**, 333–358.

Hutchins, Nicholas, Nickels, Timothy B, Marusic, Ivan & Chong, MS 2009 Hot-wire spatial resolution issues in wall-bounded turbulence. *Journal of Fluid Mechanics* **635**, 103–136.

Leonardi, Stefano & Castro, Ian P 2010 Channel flow over large cube roughness: a direct numerical simulation study. *Journal of Fluid Mechanics* **651**, 519–539.

Ligrani, PM & Bradshaw, P 1987 Spatial resolution and measurement of turbulence in the viscous sublayer using subminiature hot-wire probes. *Experiments in Fluids* **5** (6), 407–417.

MacDonald, M, Chan, L, Chung, D, Hutchins, N & Ooi, A 2016 Turbulent flow over transitionally rough surfaces with varying roughness densities. *Journal of Fluid Mechanics* **804**, 130–161.

Medjnoun, Takfarinas, Vanderwel, Christina & Ganapathisubramani, Bharathram 2018 Characteristics of turbulent boundary layers over smooth surfaces with spanwise heterogeneities. *Journal of Fluid Mechanics* **838**, 516–543.

Monty, JP, Dogan, E, Hanson, R, Scardino, AJ, Ganapathisubramani, B & Hutchins, N 2016 An assessment of the ship drag penalty arising from light calcareous tubeworm fouling. *Biofouling* **32** (4), 451–464.

Napoli, E, Armenio, Vincenzo & De Marchis, M 2008 The effect of the slope of irregularly distributed roughness elements on turbulent wall-bounded flows. *Journal of Fluid Mechanics* **613**, 385–394.

Nugroho, Setyo, Nugroho, Bagus, Fusil, Eric & Chin, Rey 2023 Effects of varied roughness coverage area on drag in a turbulent boundary layer using numerical simulations. *Ocean Engineering* **287**, 115721.

Perry, AE & Joubert, PN 1963 Rough-wall boundary layers in adverse pressure gradients. *Journal of Fluid Mechanics*

17 (2), 193–211.

Perry, AE & Li, J Ds 1990 Experimental support for the attached-eddy hypothesis in zero-pressure-gradient turbulent boundary layers. *Journal of Fluid Mechanics* **218**, 405–438.

Perry, Anthony Edward, Schofield, William H & Joubert, Peter N 1969 Rough wall turbulent boundary layers. *Journal of Fluid Mechanics* **37** (2), 383–413.

Sarakinos, Sotirios & Busse, Angela 2022 Investigation of rough-wall turbulence over barnacle roughness with increasing solidity using direct numerical simulations. *Physical Review Fluids* **7** (6), 064602.

Schultz, MP & Myers, A 2003 Comparison of three roughness function determination methods. *Experiments in fluids* **35**, 372–379.

Squire, DT, Morrill-Winter, C, Hutchins, N, Schultz, MP, Klewicki, JC & Marusic, I 2016 Comparison of turbulent boundary layers over smooth and rough surfaces up to high reynolds numbers. *Journal of Fluid Mechanics* **795**, 210–240.

Womack, Kristofer M, Volino, Ralph J, Meneveau, Charles & Schultz, Michael P 2022 Turbulent boundary layer flow over regularly and irregularly arranged truncated cone surfaces. *Journal of Fluid Mechanics* **933**, A38.